SUPPLEMENTAL MATERIALS AND METHODS

Ploidy determination by flow cytometry

Flow cytometry was used to verify the haploid DNA content of each strain for which an image is shown in the manuscript. Protocols for ploidy determination by DNA content using flow cytometry were adapted from published methods (1, 2). To rule out the possibility of self-diploidization, the DNA content of known haploid (BY4741) and diploid (BY4743) strains were compared to F45 background strains. All F45 background strains used in morphology assays showed peaks corresponding to haploid DNA content. The relatively small 1N peak and peak near 750 in our F45 background strains are very likely due to cell clumping, with this effect being stronger in the more flocculent F45 fluffy strain (Fig. S2). This effect is similar to published observations in other non-laboratory strains (3). The histograms shown are representative of gated cell populations, and the scatter plots show the gates applied.

DIG1 plasmid construction

Plasmid pAB340 was constructed by cloning *DIG1* and the surrounding intergenic region into a centromere plasmid with a G418 resistance marker. *DIG1* and its native promoter were cloned from BY4741 using the following primers into vector pFA6a-*KanMX4* (4) utilizing Clontech In-Fusion HD cloning kit following the manufacturer's protocol.

DIG1_infusionconstr3_F: 5'- GAATTCATCGATGATGCTCTTTTAAATTCTTCTGTTTG-3'
DIG1_infusionconstr3_R: 5'- ACTAGTGGATCTGATCAATAACAAGGAGGGAAGACCA-3'

The empty pFA6a-*KanMX4* vector (AB352) was used as the control plasmid for comparative growth and phenotype experiments.

Molecular karyotyping by RAD-seq coverage

Processing raw sequencing data

For each lane of sequencing, the raw reads were separated into bins based on their 4-base strain-specific barcode (5' end of each read). Within each strain-specific bin the barcodes were removed and reads were then aligned to the S288c reference genome sequence (SGD R64-1-1_20110203) using BWA (v0.5.8) (5) with up to 6 mismatches allowed. The 5' start positions of all reads with a Phred-scaled mapping alignment quality of at least 20 were counted, resulting in a set of marker positions for each strain along with the number of reads aligning to each of those positions.

Marker selection

Next, a series of filtering steps were performed to select an optimal set of markers to represent the DNA copy number across the genome. First, markers with a median of 0 or 1 counts over all strains sequenced for this study (~400) were removed. We believe that the majority of these markers represent sequencing or DNA fragmentation errors. Second, the consistency of the markers was compared to the expected length of the *Mfe*I-*Mbo*I DNA fragment, based on the S288c reference sequence, i.e. each marker should represent a set of reads directed to the *Mfe*I end of a unique *Mfe*I-*Mbo*I restriction fragment.

For each marker within each strain, the proportion of all reads aligning to that marker was then calculated, as follows:

$$Marker\ proportion = \frac{Marker\ count}{Total\ read\ counts\ for\ strain}$$

The consistency of each marker was then expressed as the Coefficient of Variance (CV) of those proportions across all strains and plotted against the predicted marker fragment length (Fig. S10).

As can be seen from the figure, the CV of markers arising from fragments well within the expected gel-selected size range (~75-425 bp) is low, but rises rapidly outside this range. In addition, a small number of markers within the selected size range still have inconsistent behavior (high CV). We therefore decided to set 2 filters, 125bp <= Marker fragment length <= 400bp, and Marker CV <= 0.6, to select for markers that we believe should behave in a reliable manner.

$$Markers_{Length\ and\ C.V. filtered} = Marker\ if\ (125bp \leq Marker\ Length \leq 400bp \cap C.V. \leq 0.6)$$

This reduces the markers available for the subsequent analysis by about 30%, but still leaves more than 3000 markers spanning the genome.

Individual strain calculations relative to the euploid reference panel

To normalize marker-specific coverage effects, a reference euploid panel (R.E.P.) of 13 sequenced strains was selected. For each marker in each query strain the read coverage (proportion) was normalized using the mean read coverage (proportion) from this panel. Assessment of the copy number of each chromosome in each query strain was then carried out as follows. First, for each marker in the length and CV filtered set, the proportion of all reads aligning to the marker was calculated and then normalized by dividing by the mean marker proportion from the reference euploid panel:

$$Marker\ ratio = \frac{Marker\ proportion}{Mean\ marker\ proportion\ of\ R.E.P.}$$

As this ratio will vary slightly depending on ploidy (aneuploids versus euploids or other aneuploids), it was then normalized to set the median marker ratio to 1:

$$Marker\ ratio_{Query\ strain\ normalized} = \frac{Marker\ ratio}{Median\ marker\ ratio\ for\ query\ strain}$$

The resulting normalized marker ratios were then plotted on a $\log_2$ scale against the marker number, ordered according to the genomic position, using the R statistical software environment (http://www.r-project.org/). Each point represents a marker, and chromosomes are given alternating colors. To keep a constant scale, the y-axis was limited from the values of -1 to 2. The ratios of an extremely small number of markers lie outside this range, but do not affect the interpretation of the figures. These plots, in conjunction with flow cytometry analysis, were then used to assess the number of copies of each chromosome in each strain.

Growth assays in liquid and solid media

The growth behaviors of fluffy and smooth strains were compared in liquid versus solid media. Liquid growth for F45, YO785, YO1770/YO1771 (2 independent transformants of F45 containing the empty vector pFA6a-kanMX4), and YO1772/YO1773 (2 independent transformants of F45 containing the *DIG1* CEN plasmid pAB340) was measured using a Tecan Sunrise instrument with Magellan 6 software. Overnight cultures of strains were sonicated to separate large cell clumps and were counted using a hemocytometer. Cultures were seeded in treated 96-well plates at a density of 10^5 cells/ ml in a well volume of 150 µl. Plates were incubated with continuous shaking and OD_{600} readings were taken every 15 minutes until saturation. F45 was compared to the chromosome XVI disome (YO785) in YPD while the overexpressed *DIG1* smooth strains (YO1772/ YO1773) were compared with the F45 plus empty vector (YO1770/YO1771) in YPD + G418 media. Despite agitation YO1770 and YO1771 clumped at the edges of the wells, so a final OD_{600} measurement was taken at the end of the growth following resuspension. Multiple

replicates of each strain (25-30 wells) were measured across 2 runs. Outlying wells were excluded from subsequent analysis. Additionally, liquid growth OD_{600} to cell count comparison was established on a per-strain basis at 1:4, 1:16, 1:64, and 1:256 dilutions. From the resulting growth curves (Fig. S11*A*, *B*) we extracted the instantaneous growth rates (Fig. S11*C*, *D*) by assuming exponential growth for all four strains for each time step.

For the solid media growth time courses, single cells were spotted to solid media using a BD FACSAria II in a "checkerboard" layout of 48 cells and 12.7 mm spacing between cells. Five plates of each strain were prepared in this fashion. After spotting, one plate from each strain was placed face-up without lid, and a sheet of 0.25" thick clear acrylic was weighted down over these four plates to prevent contamination and desiccation. These plates were imaged every 15 minutes from day 1 through day 4 of growth. Five images were taken at each time point, and the five images were averaged to decrease noise. The F45 and YO785 plates were imaged side-by-side with one camera, and YO1770 and YO1772 plates were imaged side-by-side with a second camera. Images of each plate were segmented using ImageJ (http://rsb.info.nih.gov/ij/) to extract colony area from each image (Fig. S12). The rate of growth in each replicate was calculated by dividing the difference in area between successive timepoints by the elapsed time. These rates were then smoothed using an 11-element moving average window, and the maximum rates for all replicates were calculated and averaged (Fig. 6*C*, 6*D*). To obtain cell counts per colony, representative colonies (20 per strain) were scraped from the plates and resuspended in 1 ml of PBS at the end of day 4. OD_{600} of these cell suspensions were measured using a Tecan Sunrise at dilutions of 0, 1:4, 1:16, 1:64, and 1:256. Cells from two colonies per strain were also counted (at each dilution) using a hemocytometer to establish the relationship between OD_{600} and cell number for each strain and to obtain total cells per colony (Fig. 6*E*, 6*F*).

Curing prions from strains

To cure our strains of prions in two different ways, we grew our strains in liquid YPD media containing 1 mM Guanidine Hydrochloride (GuHCl) for 24 hours and on YPD + 4mM GuHCl agar plates for 3 days (6). Following GuHCl treatment, cells were streaked or plated out onto YPD agar plates for assessment of colony morphology (Fig. S1).

SUPPLEMENTAL INFORMATION TEXT

Unstable and inviable strains

Because colony morphology can be influenced by the media conditions, it is not possible to assay the trait on every medium. For example, on minimal media (such as those used for the His^+ Ura^+ selection for disomes and 5-FOA counter selection against disomes) the fluffy morphology is much less pronounced (even in the original euploid strain) making it difficult to distinguish smooth and fluffy. We therefore pick a relatively large number of random colonies to phenotype on the "assay medium" (rich medium, YPD)—because we cannot see the trait on minimal medium when we pick the colonies, the choice of colonies is truly random. When all of the chosen colonies showed a similar morphology, we RAD sequenced a subset to confirm that they have the correct karyotype. In cases, where there was more than one phenotypic class, we picked both classes (below). The only exception is a class of spontaneously arising mitochondrial mutants that are incapable of forming fluffy colonies (regardless of karyotype). While these arise at high frequency in this (and some other) strain backgrounds, they are easily distinguished by colony color and in ability to grow on respiratory carbon sources (below).

In the F45 strain background disomies II, VI, XI and XIII were too unstable and variable to assay colony morphology confidently. Induced disomies II and XI grew poorly on selective media following induction and nearly all colonies were respiratory deficient on glycerol media.

Representative isolates were checked for karyotype but were not analyzed for colony morphology. RAD-seq analysis revealed that nearly all disomy II and XI candidates had either picked up additional whole or partial chromosomes, or were displaying highly unstable karyotypes. Disomy VI strains grew on selective media and had *respiratory positive* candidates, but the RAD-seq analysis revealed most candidates had either picked up additional whole or partial chromosomes, or were displaying highly unstable karyotypes. Finally, disomy XIII has a marginally more stable karyotype, but because the strains become respiratory deficient at such a high rate, it was extremely difficult to maintain a *respiratory positive* line. Although YPD was used as the primary colony morphology assay medium it was observed that, unlike the other F45 background strains, the chromosome XIII disomes were extremely fluffy on synthetic media, despite the prevalence of respiratory deficient cells. Although we have not confirmed them molecularly, the high rates of respiratory deficiency are consistent with instability of the mitochondrial genome, which can be induced by perturbations in numerous nuclear encoded genes such as components of the mitochondrial ribosome (7). We speculate that this may be another trait affected by the copy number imbalance seen in aneuploid strains.

Interestingly, in many of the less stable aneuploid isolates we saw an additional gain of chromosome XV while being held on selective media (SC-Ura-His). Karyotyped isolates from disomy II, VIII, XI and XII construct backgrounds all had a significant number of XV double disomies upon karyotyping directly from selective media (Table S2). In the cases of disomies VIII and XII many of the isolates that were karyotyped following growth on YPD (the morphology assay medium) had lost the additional XV but maintained their induced disomy. Additionally, in our strain background nearly all induced and karyotyped disomy IV strains also gained a copy of chromosome VII, which was stable even on YPD.

There is a difference in the aneuploid strains that we consistently recover as compared to previous studies (8, 9). While those authors were unable to recover strains disomic for chromosome VI, we were unable to recover strains stably disomic for chromosomes II, VI and XI. We believe that this could be explained by the allelic differences present in the different strain backgrounds, leading to viability differences of the aneuploids. These results underscore the role that genetic variation plays in the phenotypic variation of aneuploids and, by extrapolation, the phenotypic variability seen in some diseases linked to aneuploidy.

Isolation of smooth colony strains

In our screen for smooth variants, we obtained 14 smooth isolates from a combination of the original F45 strain and some fluffy revertants (F45 "2nd gen") from F45 Smooth. 7 of the 14 were disomic strains, while the remaining strains show no discernible change in karyotype. These non-disomic smooth variants may have resulted from mutations, and were not followed up further.

Gene specific dosage imbalance

To test whether the colony morphology phenotypic toggle is in fact modulated by the copy number variation of specific genes, we transformed the original F45 (fluffy) strain with a set of low copy plasmids containing portions of chromosome XVI (10). A plasmid containing 10.8 kb of chromosome XVI, including seven full-length and two partial open reading frames, was able to confer the smooth state (Fig. S9*A*). We then determined which gene(s) on the plasmid were responsible for altering the phenotype by two methods. First, we deleted one copy of each of the nine genes (individually) in the context of an otherwise complete XVI disome (Fig. S13). Our results (Fig. S9*B*) demonstrate that restoring the copy number of only *DIG1* restored a fluffy phenotype, although not to the original shape. Second, we increased the copy number of only *DIG1* by introducing it into the euploid fluffy strain (F45) on a low copy number plasmid and found that it was able to confer the smooth phenotype (Fig. 6*B*). However, the intermediate phenotype

obtained by restoring *DIG1* copy number in the context of the XVI disomy supports the hypothesis that additional genes on chromosome XVI contribute to the phenotypic switch.

SUPPLEMENTARY TABLES

Table S1 | *S. cerevisiae* strains imaged in this study. With the exception of YO795, YO796, YO880 and YO881, all strains are derivatives of F45.

Strain Name	Genotype	Karyotype
F45	MAT**a** *hoΔ::HphMX6*, *SPS2:EGFP:NatMX4*, serine auxotroph	Euploid haploid
YO486[1]	*SPS2:EGFP:kanMX4, hoΔ::HphMX6*	Disomy I, naturally occuring
YO502[2]	*SPS2:EGFP:NatMX4*, *hoΔ::HphMX6*	Euploid haploid
YO785	MAT**a** *hoΔ::HphMX6*, *SPS2:EGFP:NatMX4*, serine auxotroph	Disomy XVI, naturally occurring
YO885[7]	MAT**a** *hoΔ::HphMX6*, *SPS2:EGFP:NatMX4*, serine auxotroph	Euploid haploid, obtained from YO785
YO903	MAT**a** *hoΔ::HphMX6*, *SPS2:EGFP:NatMX4*, serine auxotroph	Disomy XV, naturally occurring
YO904	MAT**a** *hoΔ::HphMX6*, *SPS2:EGFP:NatMX4*, serine auxotroph	Disomy III, naturally occurring
YO958	MAT**a** *hoΔ::HphMX6*, *SPS2:EGFP:NatMX4*, serine auxotroph	Disomy X, naturally occurring
YO963	MAT**a** *hoΔ::HphMX6*, *SPS2:EGFP:NatMX4*, serine auxotroph	Disomy V, naturally occurring
YO983	MAT**a** *hoΔ::HphMX6*, *SPS2:EGFP:NatMX4*, serine auxotroph	Euploid haploid, obtained from YO903
YO987	MAT**a** *hoΔ::HphMX6*, *SPS2:EGFP:NatMX4*, serine auxotroph	Euploid haploid, obtained from YO904
YO1015	MAT**a** *hoΔ::HphMX6*, *SPS2:EGFP:NatMX4*, ura3Δ0, his3Δ*::KanMX4*, *cen16Δ::*P_{GAL1}*-CEN3-ura3::HIS3*, serine auxotroph	Euploid haploid
YO1064	MAT**a** *hoΔ::HphMX6*, *SPS2:EGFP:NatMX4*, *ura3Δ0*, *his3Δ::KanMX4*, *cen16Δ::* P_{GAL1}*-CEN3-ura3::HIS3/cen16Δ::* P_{GAL1}*-CEN3-URA3*, serine auxotroph	Disomy XVI, conditional centromere
YO1099	MAT**a** *hoΔ::HphMX6*, *SPS2:EGFP:NatMX4*, *ura3Δ0*, *his3Δ::KanMX4*, *cen16Δ::* P_{GAL1}*-CEN3-ura3::HIS3*, serine auxotroph	Euploid haploid, “2nd Gen”
YO1451	MAT**a** *hoΔ::HphMX6*, *SPS2:EGFP:NatMX4*, serine auxotroph	Euploid haploid, obtained from YO958
YO1474	MAT**a** *hoΔ::HphMX6*, *SPS2:EGFP:NatMX4*, serine auxotroph	Euploid haploid, obtained from YO963
YO1496	MAT**a** *hoΔ::HphMX6*, *SPS2:EGFP:NatMX4*, *ura3Δ0*, *his3Δ::KanMX4*, *cen1Δ::* P_{GAL1}*-CEN3-ura3::HIS3/cen1Δ::* P_{GAL1}*-CEN3-URA3*, serine auxotroph	Disomy I, conditional centromere
YO1497	MAT**a** *hoΔ::HphMX6*, *SPS2:EGFP:NatMX4*, *ura3Δ0*, *his3Δ::KanMX4*, *cen4Δ::* P_{GAL1}*-CEN3-ura3::HIS3/cen4Δ::* P_{GAL1}*-CEN3-URA3*, serine auxotroph	Disomy IV conditional centromere, + VII naturally occurring
YO1505	MAT**a** *hoΔ::HphMX6*, *SPS2:EGFP:NatMX4*, *ura3Δ0*, *his3Δ::KanMX4*, *cen7Δ::* P_{GAL1}*-CEN3-ura3::HIS3/cen7Δ::* P_{GAL1}*-CEN3-URA3*, serine auxotroph	Disomy VII, conditional centromere

YO1510	MAT**a** *hoΔ::HphMX6*, *SPS2:EGFP:NatMX4*, *ura3Δ0*, *his3Δ::KanMX4*, *cen8Δ:: P_{GAL1}-CEN3-ura3::HIS3/cen8Δ:: P_{GAL1}-CEN3-URA3*, serine auxotroph	Disomy VIII, conditional centromere
YO1532	MAT**a** *hoΔ::HphMX6*, *SPS2:EGFP:NatMX4*, *ura3Δ0*, *his3Δ::KanMX4*, *cen9Δ:: P_{GAL1}-CEN3-ura3::HIS3/cen9Δ:: P_{GAL1}-CEN3-URA3*, serine auxotroph	Disomy IX, conditional centromere
YO1533	MAT**a** *hoΔ::HphMX6*, *SPS2:EGFP:NatMX4*, *ura3Δ0*, *his3Δ::KanMX4*, *cen9Δ:: P_{GAL1}-CEN3-ura3::HIS3/cen9Δ:: P_{GAL1}-CEN3-URA3*, serine auxotroph	Disomy IX conditional centromere, + III naturally occurring
YO1542	MAT**a** *hoΔ::HphMX6*, *SPS2:EGFP:NatMX4*, *ura3Δ0*, *his3Δ::KanMX4*, *cen12Δ:: P_{GAL1}-CEN3-ura3::HIS3/cen12Δ:: P_{GAL1}-CEN3-URA3*, serine auxotroph	Disomy XII conditional centromere, + XV naturally occurring
YO1543	MAT**a** *hoΔ::HphMX6*, *SPS2:EGFP:NatMX4*, *ura3Δ0*, *his3Δ::KanMX4*, *cen12Δ:: P_{GAL1}-CEN3-ura3::HIS3/cen12Δ:: P_{GAL1}-CEN3-URA3*, serine auxotroph	Disomy XII conditional centromere, XV gained then lost naturally
YO1546	MAT**a** *hoΔ::HphMX6*, *SPS2:EGFP:NatMX4*, *ura3Δ0*, *his3Δ::KanMX4*, *cen13Δ:: P_{GAL1}-CEN3-ura3::HIS3/cen13Δ:: P_{GAL1}-CEN3-URA3*, serine auxotroph	Disomy XIII, conditional centromere
YO1548	MAT**a** *hoΔ::HphMX6*, *SPS2:EGFP:NatMX4*, *ura3Δ0*, *his3Δ::KanMX4*, *cen14Δ:: P_{GAL1}-CEN3-ura3::HIS3/cen14Δ:: P_{GAL1}-CEN3-URA3*, serine auxotroph	Disomy XIV, conditional centromere
YO795[3]	*SPS2:EGFP:NatMX4, hoΔ::HphMX6, gal7Δ0::kanMx4*	Euploid haploid
YO796[4]	*SPS2:EGFP:NatMX4,* hoΔ::dsdAMX4, *gal7Δ0::kanMx4*	Euploid haploid
YO880[5]	MATα *SPS2:EGFP:NatMX4*, *hoΔ::HphMX6*, *gal7Δ::KanMX4* (derived from YO795 x YO796 progeny)	Disomy XVI, naturally occurring
YO881[6]	MATα *SPS2:EGFP:NatMX4 hoΔ::HphMX6 gal7Δ::KanMX4* (derived from YO880)	Euploid haploid
YO898[7]	MAT**a** *hoΔ::HphMX6*, *SPS2:EGFP:NatMX4*, serine auxotroph	Euploid haploid
YO959[7]	MAT**a** *hoΔ::HphMX6*, *SPS2:EGFP:NatMX4*, serine auxotroph	Euploid haploid
YO965[7]	MAT**a** *hoΔ::HphMX6*, *SPS2:EGFP:NatMX4*, serine auxotroph, respiratory deficient	Euploid haploid
YO971[7]	MATα *hoΔ::HphMX6*, *SPS2:EGFP:NatMX4*, ura3Δ0, serine auxotroph	Euploid haploid
YO972[7]	MATα *hoΔ::HphMX6*, *SPS2:EGFP:NatMX4*, ura3Δ0, serine auxotroph	Euploid haploid

YO977[7]	MAT**a** *hoΔ::HphMX6*, *SPS2:EGFP:NatMX4*, serine auxotroph	Euploid haploid
YO979[7]	MAT**a** *hoΔ::HphMX6*, *SPS2:EGFP:NatMX4*, serine auxotroph	Euploid haploid
YO981[7]	MAT**a** *hoΔ::HphMX6*, *SPS2:EGFP:NatMX4*, serine auxotroph	Euploid haploid
YO1101[7]	MAT**a** *hoΔ::HphMX6*, *SPS2:EGFP:NatMX4*, *ura3Δ0*, *his3Δ::KanMX4*, *cen16Δ:: P_{GAL1}-CEN3-ura3::HIS3*, serine auxotroph	Euploid haploid
YO1540[7]	MAT**a** *hoΔ::HphMX6*, *SPS2:EGFP:NatMX4*, serine auxotroph	Euploid haploid
YO1770	MAT**a** *hoΔ::HphMX6*, *SPS2:EGFP:NatMX4*, serine auxotroph, transformed with *pFA6a-KanMX4* vector (AB352), biological replicate of YO1771	Euploid haploid
YO1771	MAT**a** *hoΔ::HphMX6*, *SPS2:EGFP:NatMX4*, serine auxotroph, transformed with *pFA6a-KanMX4* vector(AB352), biological replicate of YO1770	Euploid haploid
YO1772	MAT**a** *hoΔ::HphMX6*, *SPS2:EGFP:NatMX4*, serine auxotroph, transformed with *DIG1-pFA6a-KanMX4* vector (AB340), biological replicate of YO1773	Euploid haploid
YO1773	MAT**a** *hoΔ::HphMX6*, *SPS2:EGFP:NatMX4*, serine auxotroph, transformed with *DIG1-pFA6a-KanMX4* vector (AB340), biological replicate of YO1772	Euploid haploid
F45_YSEQ127[7]	MAT**a** *hoΔ::HphMX6*, *SPS2:EGFP:NatMX4*, serine auxotroph	Euploid haploid
F45_YSEQ128[7]	MAT**a** *hoΔ::HphMX6*, *SPS2:EGFP:NatMX4*, serine auxotroph	Euploid haploid
F45_YSEQ129[7]	MAT**a** *hoΔ::HphMX6*, *SPS2:EGFP:NatMX4*, serine auxotroph	Euploid haploid

[1]Derived from UC5 (Sake) (11)
[2]Derived from DBVPG1853 (White Tecc) (12)
[3]Derived from EC-33 (“Evolution Canyon”) (13)
[4]Derived from YPS163 (Oak tree) (14)
[5]Haploid progeny derived from a cross between YO795 and YO796
[6]Derived from YO880
[7]Reference Euploid Panel

Table S2 | Initial karyotype and morphology for strains generated utilizing the conditional centromere construct and selected for initial RAD-seq analysis. Isolates for which the karyotype could not be called were omitted from this table.

Chromosome harboring the conditional centromere	Karyotype following induction (disomy unless otherwise specified)	Proportion of strains with the karyotype	Morphology post-induction
I	I I trisomy	14/18 4/18	Fluffy Fluffy
IV	IV+I IV+VII	1/9 8/9	Fluffy Intermediate
VII	VII	12/12	Smooth
VIII	VIII VIII + XV	10/13 2/13	Fluffy Fluffy
IX	IX IX + III	18/26 8/26	Fluffy Smooth
XII	XII +XV	11/11	Smooth
XIII	XIII	5/11*	Fluffy
XIV	XIV	12/12	Fluffy

*Because the post-induction isolates exhibited a range of morphologies on the selective media, several isolates of each class, fluffy and smooth, were selected for karyotyping. All fluffy isolates were confirmed chromosome XIII disomes. The smooth isolates were suspected self-diploids which is consistent with what others have seen using this conditional centromere method (8).

SUPPLEMENTARY FIGURES

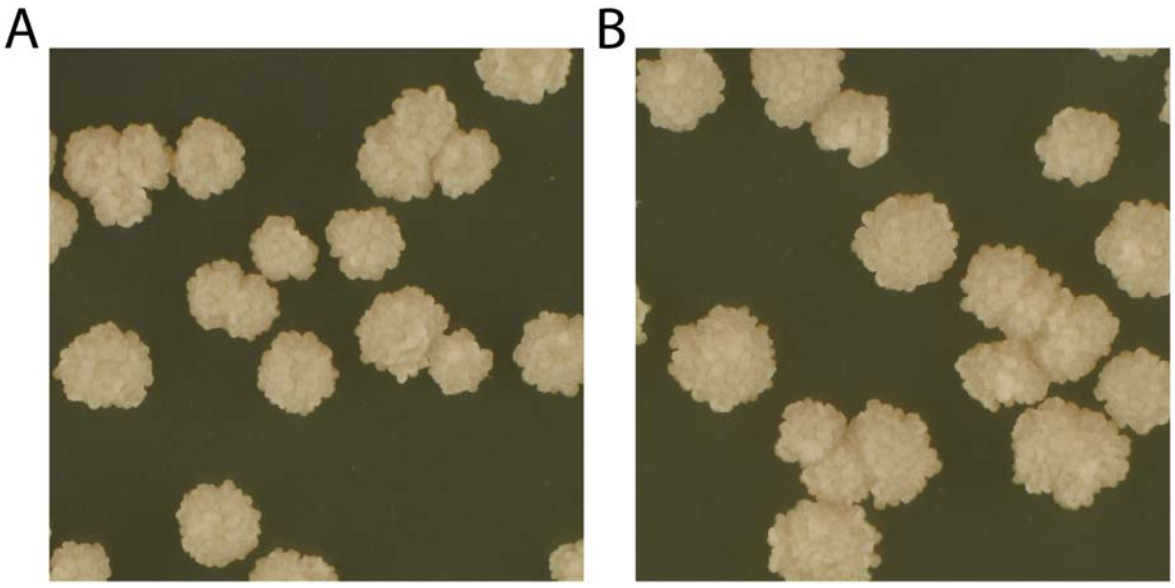

Figure S1 | Phenotypic switching for our strain is not due to prions. (*A*) F45 colonies that have been cured of prions by growth in YPD + 1mM Guanidine Hydrochloride for 24 hours. (B) F45 colonies that have not been cured of prions. Images are taken on day 3 of growth. Since the colony morphologies of both treated and untreated colonies are indistinguishable, prions are unlikely to be the mechanism underlying the switch for our strain.

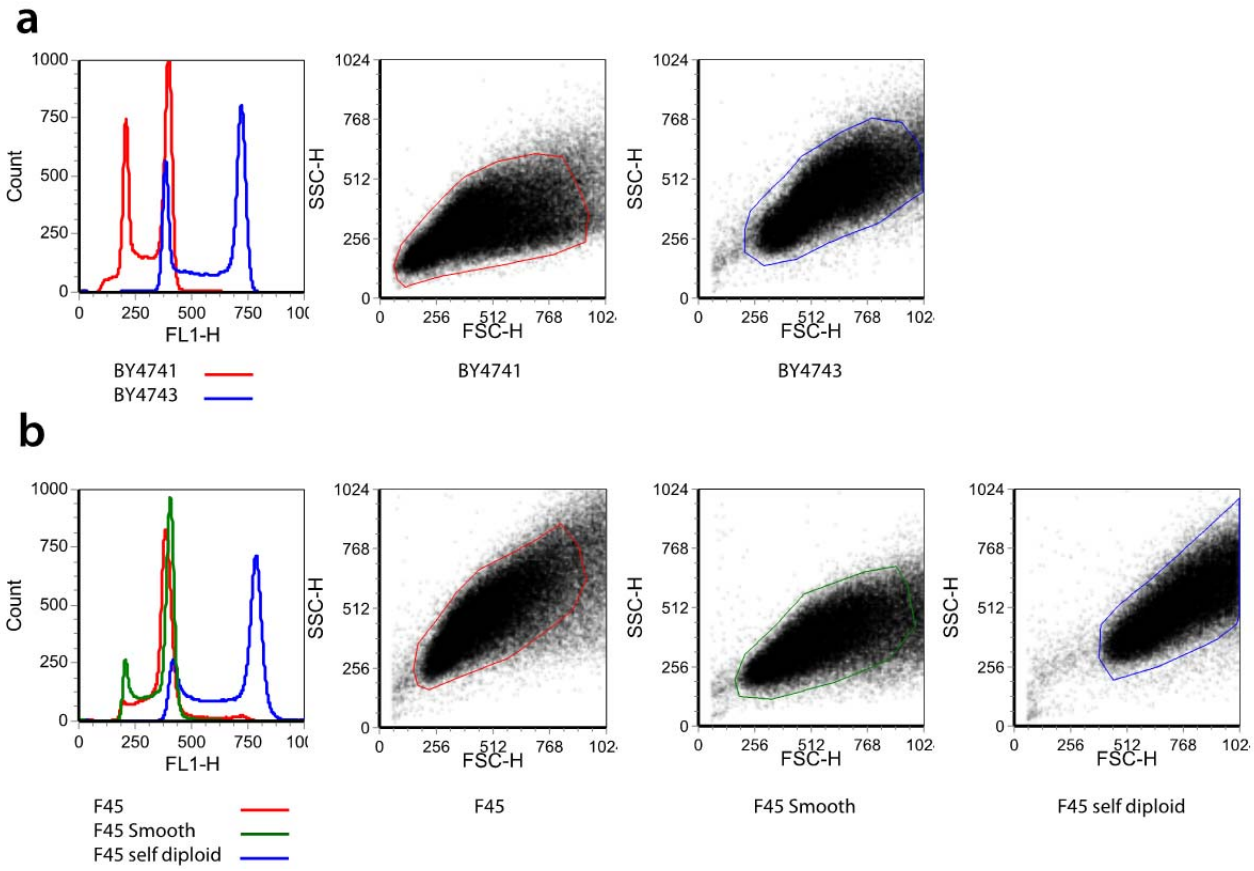

Figure S2 | DNA content assessed by flow cytometry. a) Histogram and applied gates for laboratory strain controls BY4741 (haploid, red) and BY4743 (diploid, blue) **b)** Histogram and applied gates for F45 (red), F45 Smooth (YO785, green) and an example of an F45 self-diploidized strain (blue)

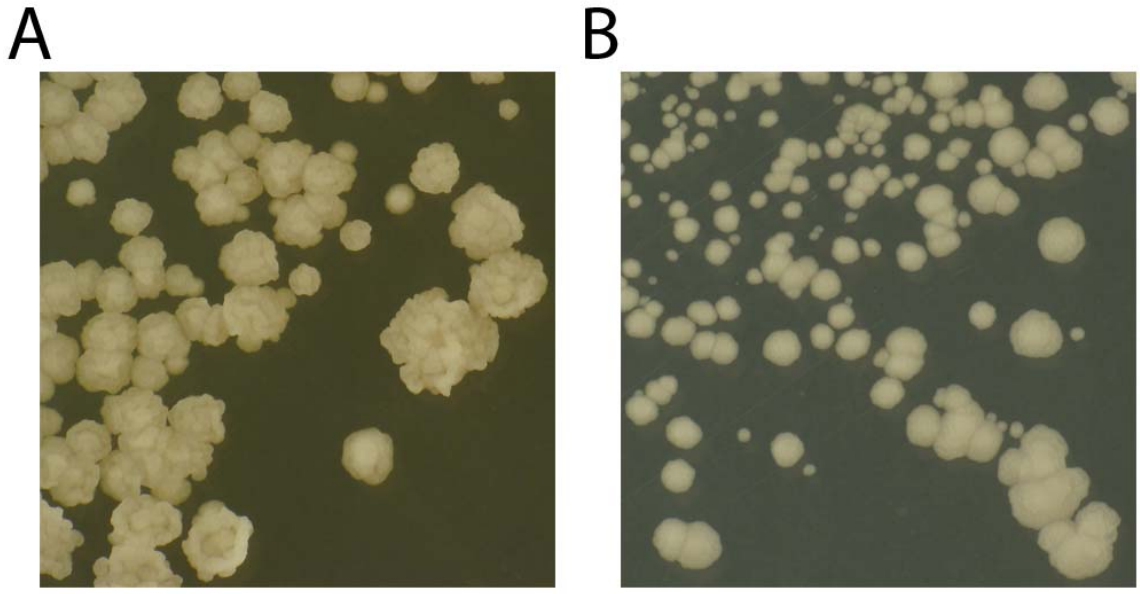

Figure S3 | Colony morphology is difficult to assess on minimal media. (*A*) Colony morphology of F45 on YPD media. (*B*) Colony morphology of F45 on minimal media (SC – Ura). Both images were taken on day 2 of growth.

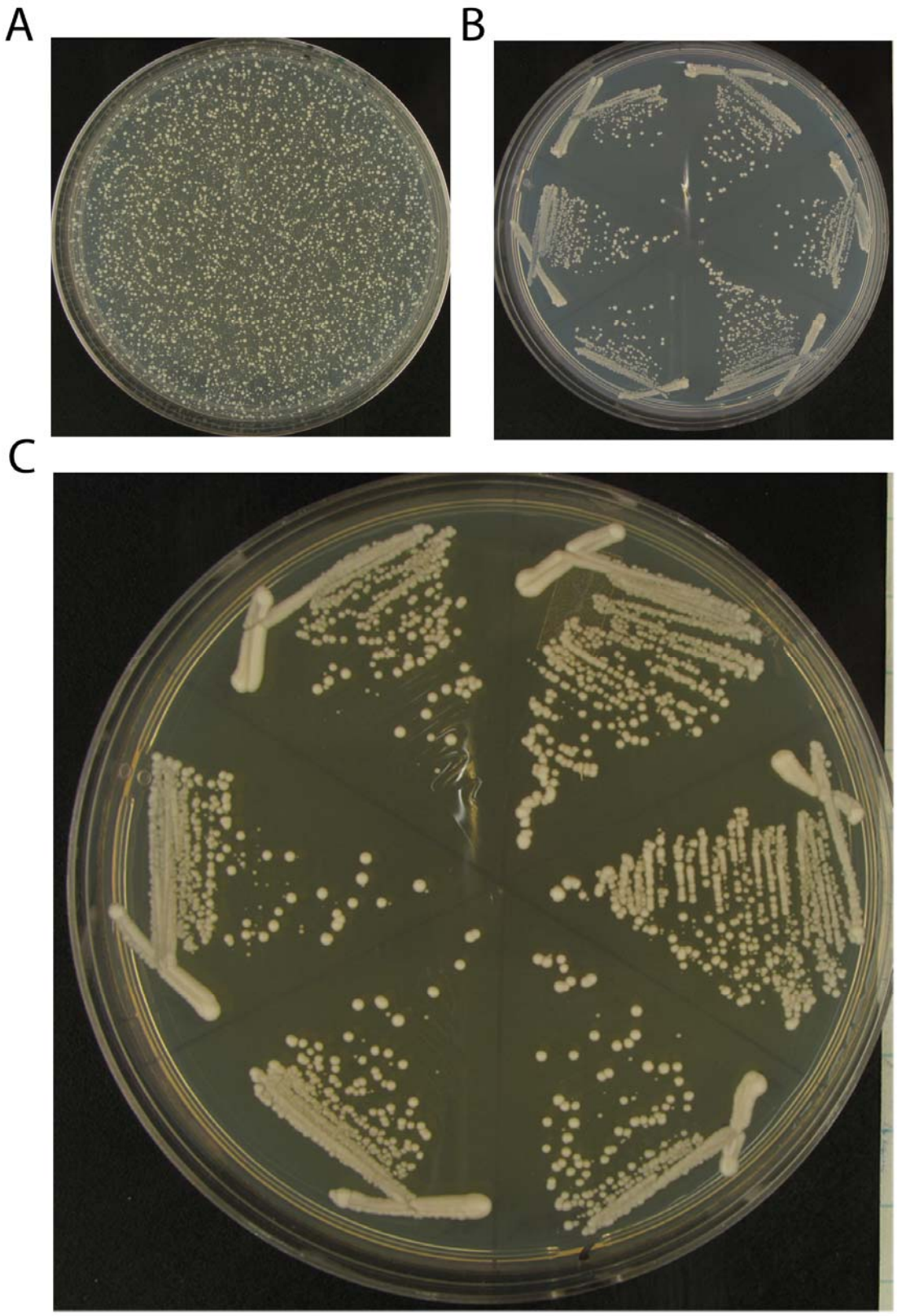

Figure S4 | Selection of disomic strains. (*A*) Representative image of initial selection plates (SC –His –Ura). As colonies were too dense, they were streaked for single colonies (*B*) Representative single colony streaks of colonies (on repeated selection plates (SC –His –Ura)) from initial selection plate. (*C*) Representative single colony streaks of single colonies (on YPD plates) from repeated selection plates, showing the smooth colony morphology of the colonies. All images are taken on day 2 of growth.

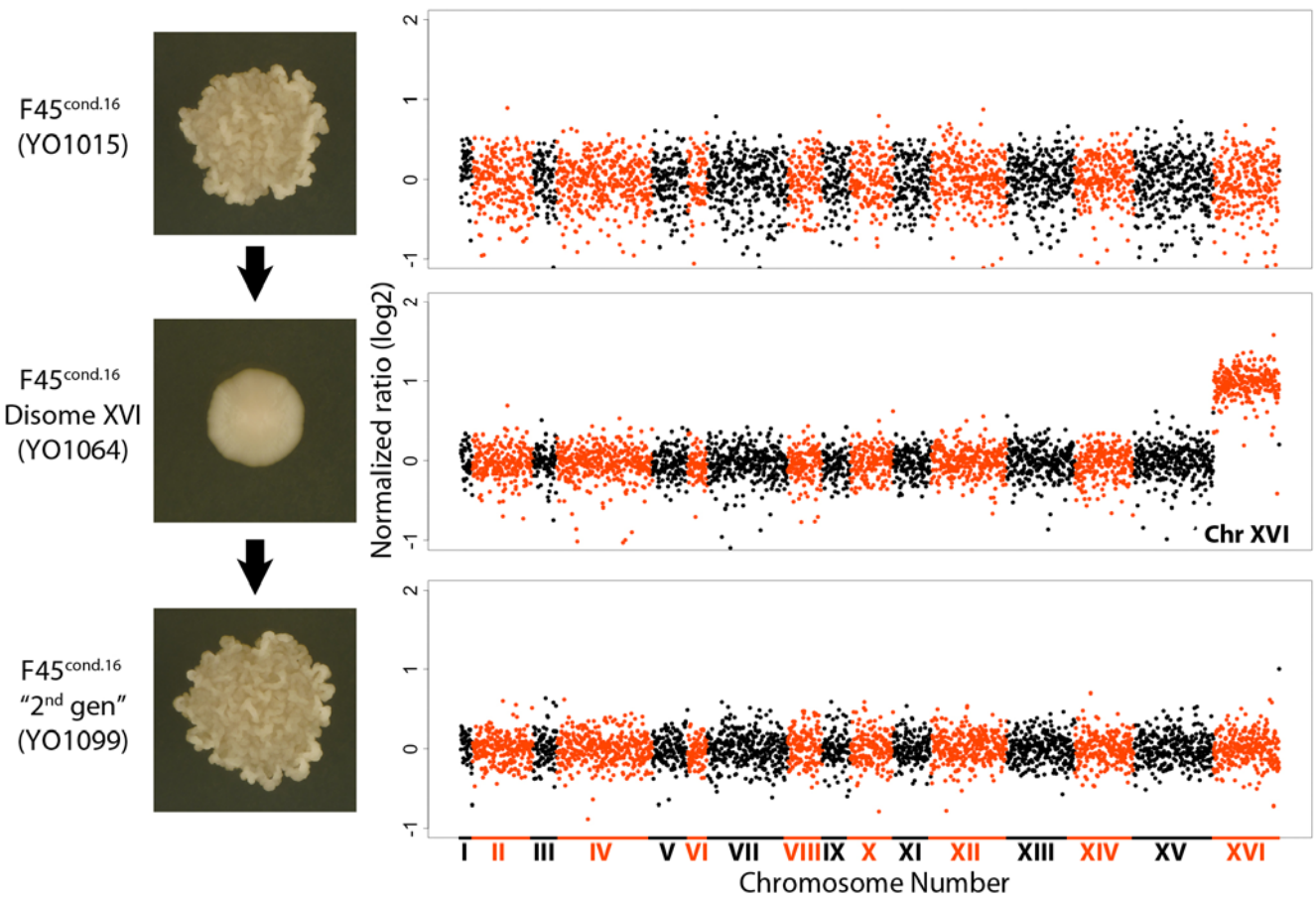

Figure S5 | Change in morphology associated with the gain and loss of chromosome XVI (containing the conditional centromere). Images are typical of observed morphology, and are taken after 4 days of growth of a single cell. Accompanying plots show the gain and loss of chromosome XVI as identified by RAD-seq and are representative of biological replicates.

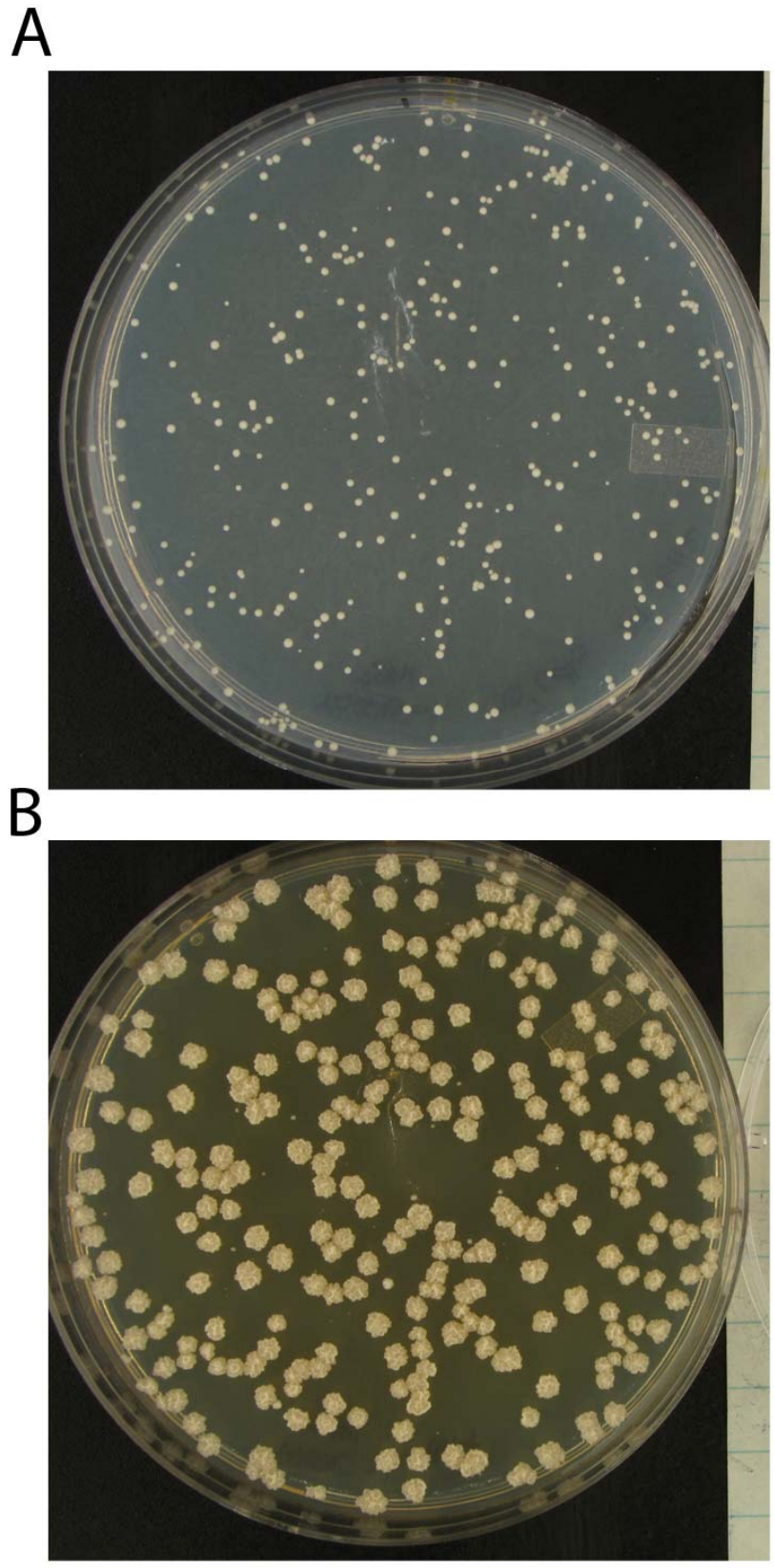

Figure S6 | Selection of euploid strains. (*A*) Representative image of initial selection plates (5-FOA). In our hands, ~10^2 out of 10^7 cells produced 5-FOA resistant colonies. As colony morphology is difficult to assess on 5-FOA plates, colonies were replica-printed onto YPD plates. (*B*) Replica-printed YPD plates, showing the fluffy colony morphology of the colonies. Images were taken on day 2 of growth.

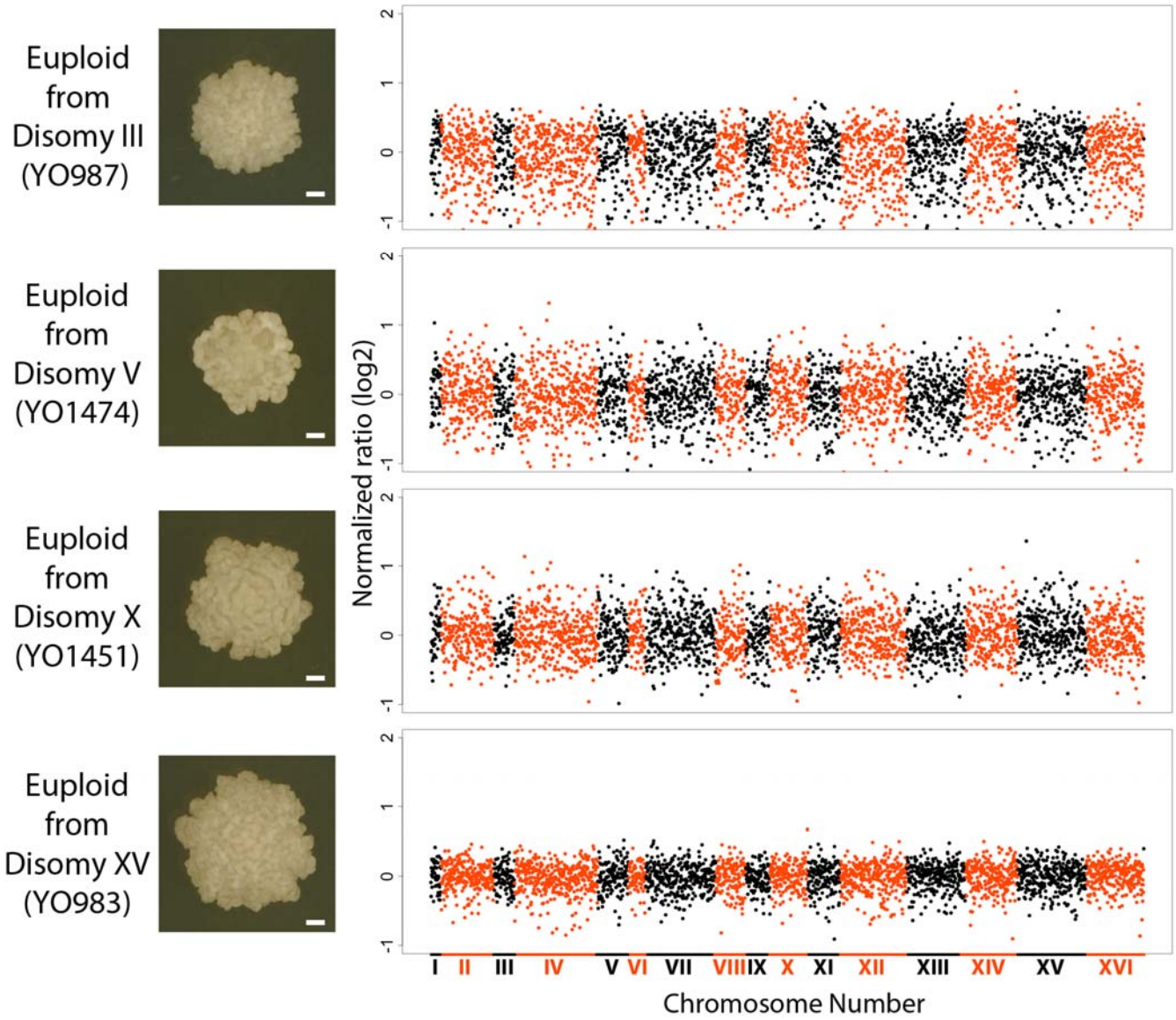

Figure S7 | Restoration of euploid karyotype returns colonies to original morphology. Images show representative colony morphology, and are taken after 3 days of growth of a single cell. Plots show restoration of euploid karyotype as identified by RAD-seq. Scale bar is 1mm.

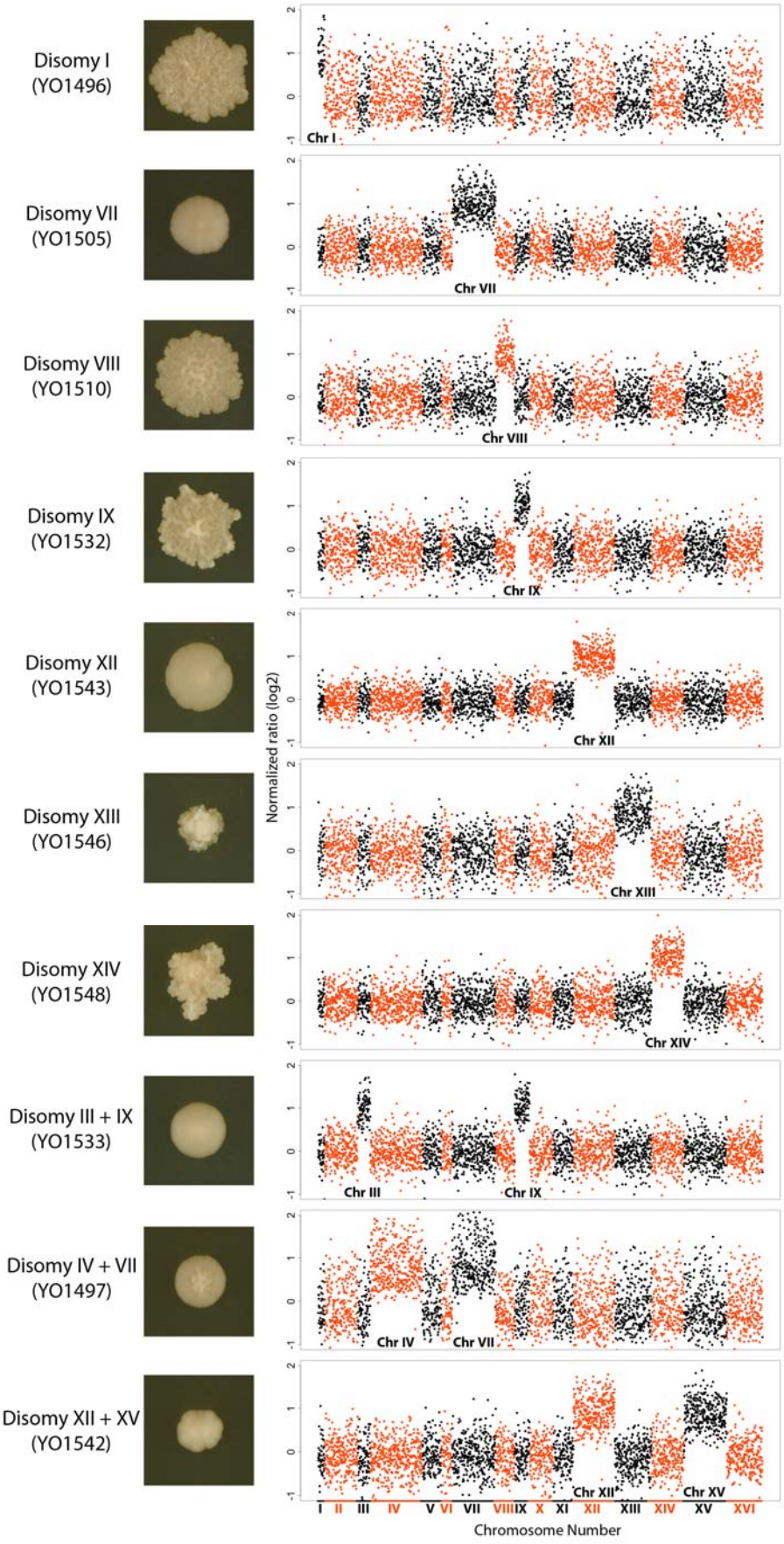

Figure S8 | Karyotypes of engineered aneuploid strains. Images show representative colony morphology, plots show the additional chromosomes as identified by RAD-seq. Images were taken on day 4 of colony growth.

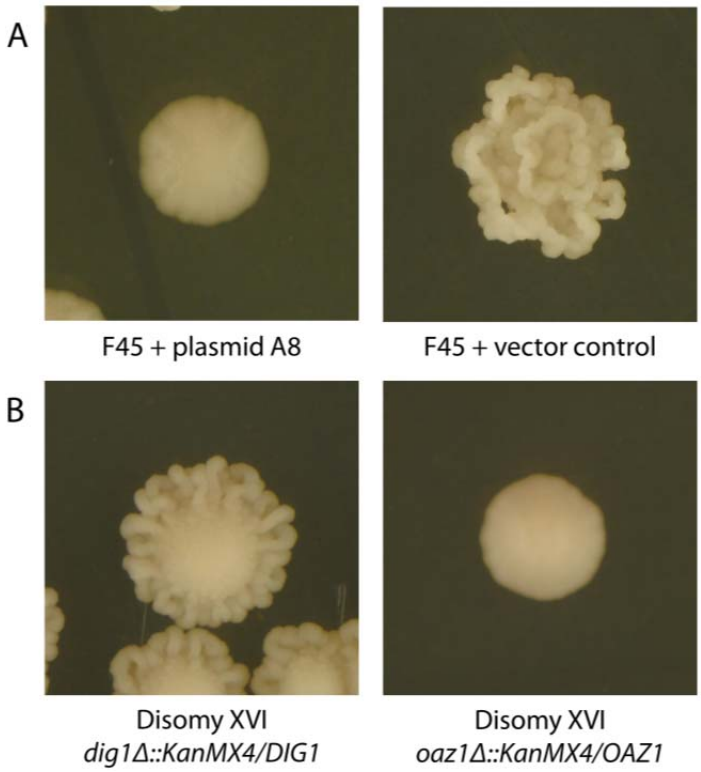

Figure S9 | *DIG1* copy number influences colony morphology. (*A*) Plasmid pGP648 containing a 10.8 kb region of chromosome XVI DNA (plasmid A8) induces a switch to the smooth phenotype in F45. Plasmid A8 contains 7 complete ORFs (*OAZ1, ARL3, MNN9, DIG1, CAM1, SGF11, ELC1*) and 2 partial ORFs (KTR6, VPS16). (*B*) Partial restoration of the fluffy phenotype is seen only in the *dig1Δ::KanMX4/DIG1* disomic XVI strain. All other knockouts remain smooth, indicating that *DIG1* is responsible for the change in morphology induced by plasmid A8.

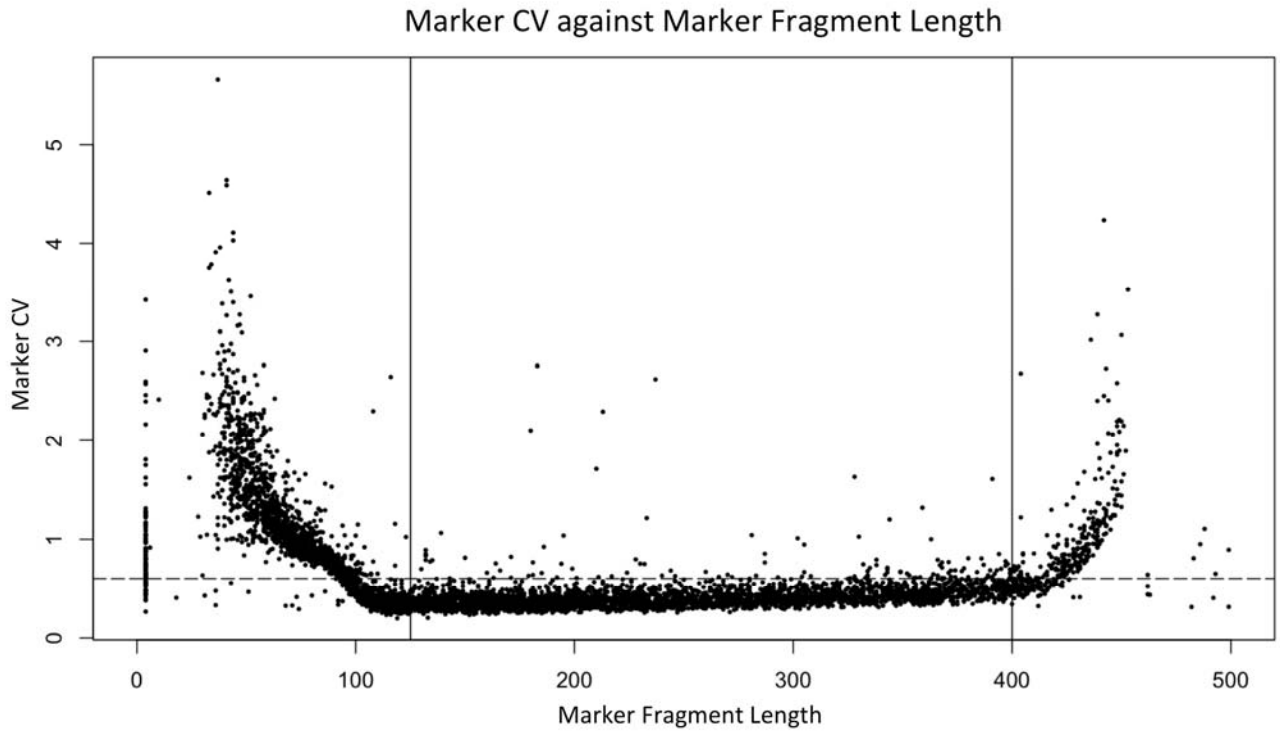

Figure S10 | Marker performance based on the predicted marker fragment length. Each point represents a marker. Lines are filters that were applied to the data, markers whose fragment lengths and CV fall in the lower middle section were used for subsequent analysis.

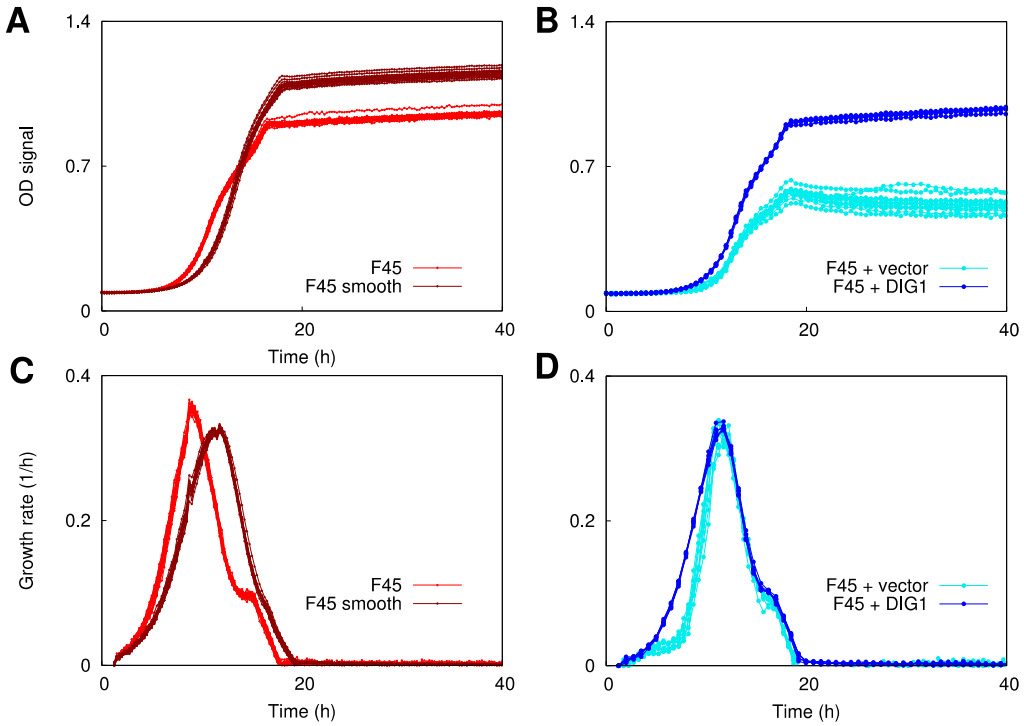

Figure S11 | Growth rates of strains in liquid media. OD (*A, B*) and growth rates (*C, D*) are plotted against time for F45 and F45 Smooth/YO785 (*A, C*); F45 + vector/YO1770 and F45 + *DIG1*/YO1772 (*C, D*).

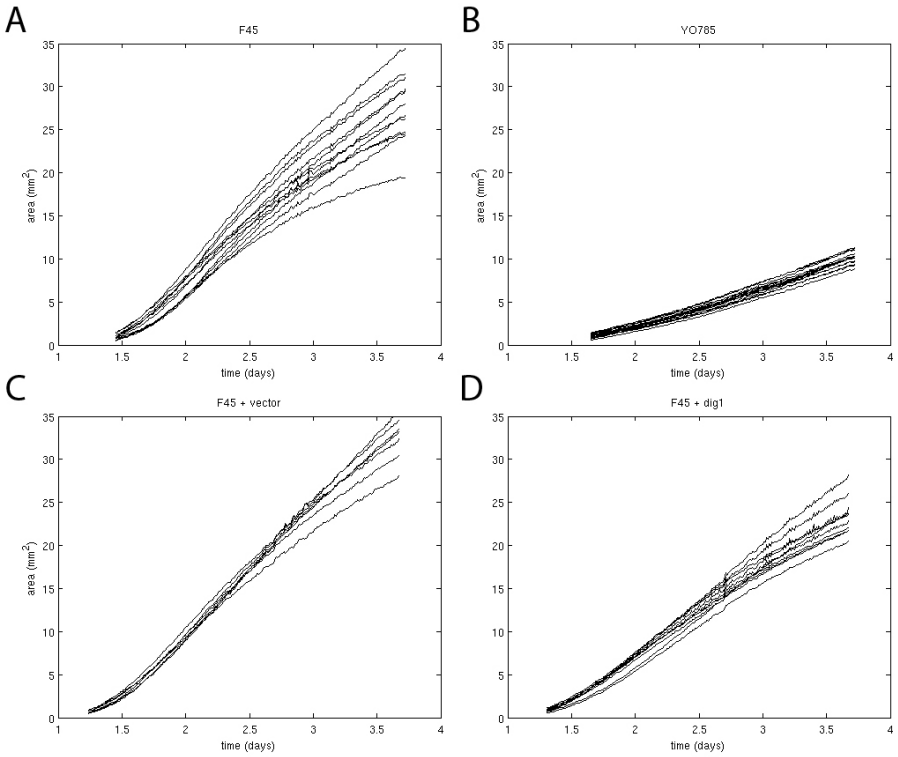

Figure S12 | Growth rates of strains on solid media. Colony area (mm^2) plotted against time (in days) for F45 (*A*), F45 Smooth/YO785 (*B*), F45 + vector/YO1770 (*C*), F45 + *DIG1*/YO1772 (*D*).

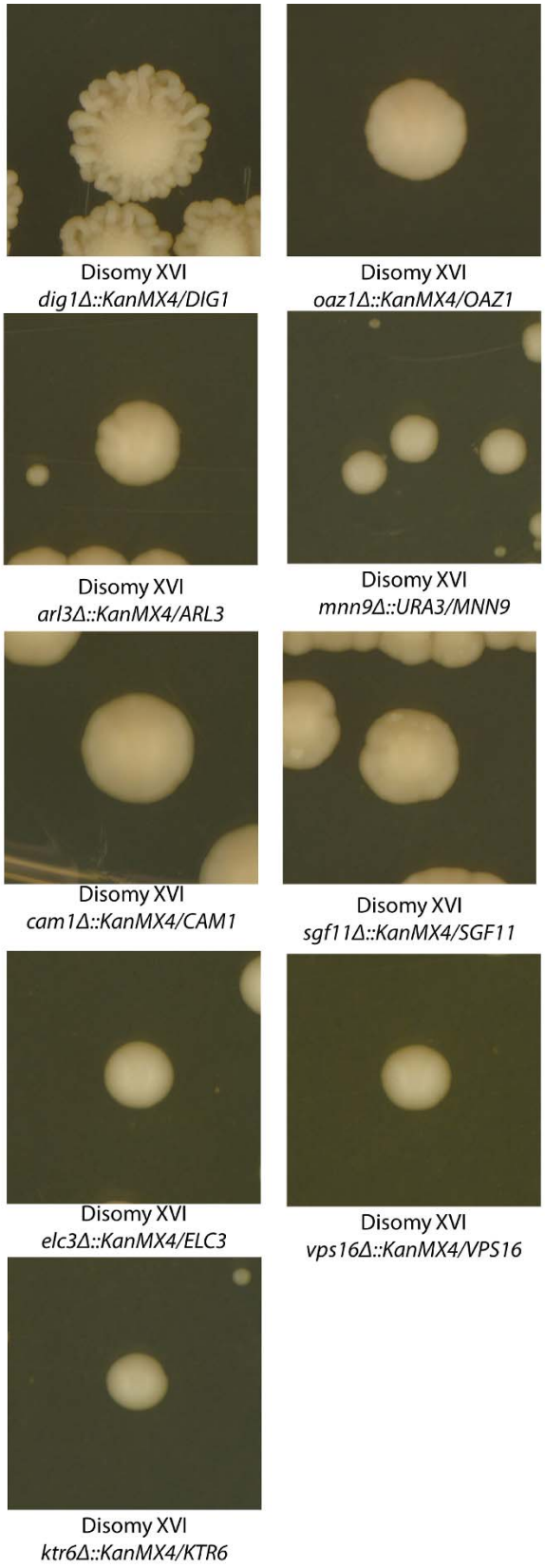

Figure S13 | Single gene deletions in the chromosome XVI disome. Only the *DIG1* deletion in the chromosome XVI disome exhibited a return to a fluffy phenotype.

References

1. Nash R, Tokiwa G, Anand S, Erickson K, & Futcher AB (1988) The WHI1+ gene of Saccharomyces cerevisiae tethers cell division to cell size and is a cyclin homolog. *Embo J* 7(13):4335-4346.
2. Haase SB & Reed SI (2002) Improved flow cytometric analysis of the budding yeast cell cycle. *Cell Cycle* 1(2):132-136.
3. Yvert G*, et al.* (2003) Trans-acting regulatory variation in Saccharomyces cerevisiae and the role of transcription factors. *Nat Genet* 35(1):57-64.
4. Wach A, Brachat A, Pohlmann R, & Philippsen P (1994) New heterologous modules for classical or PCR-based gene disruptions in Saccharomyces cerevisiae. *Yeast* 10(13):1793-1808.
5. Li H & Durbin R (2009) Fast and accurate short read alignment with Burrows-Wheeler transform. *Bioinformatics* 25(14):1754-1760.
6. Tuite MF, Mundy CR, & Cox BS (1981) Agents that cause a high frequency of genetic change from [psi+] to [psi-] in Saccharomyces cerevisiae. *Genetics* 98(4):691-711.
7. Lipinski KA, Kaniak-Golik A, & Golik P (2010) Maintenance and expression of the S. cerevisiae mitochondrial genome--from genetics to evolution and systems biology. *Biochim Biophys Acta* 1797(6-7):1086-1098.
8. Anders KR*, et al.* (2009) A strategy for constructing aneuploid yeast strains by transient nondisjunction of a target chromosome. *BMC Genet* 10:36.
9. Torres EM*, et al.* (2007) Effects of aneuploidy on cellular physiology and cell division in haploid yeast. *Science* 317(5840):916-924.
10. Hvorecny KL & Prelich G (2010) A systematic CEN library of the Saccharomyces cerevisiae genome. *Yeast* 27(10):861-865.
11. Fay JC & Benavides JA (2005) Evidence for domesticated and wild populations of Saccharomyces cerevisiae. *PLoS Genet* 1(1):66-71.
12. Liti G, Barton DB, & Louis EJ (2006) Sequence diversity, reproductive isolation and species concepts in Saccharomyces. *Genetics* 174(2):839-850.
13. Ezov TK*, et al.* (2006) Molecular-genetic biodiversity in a natural population of the yeast Saccharomyces cerevisiae from "Evolution Canyon": microsatellite polymorphism, ploidy and controversial sexual status. *Genetics* 174(3):1455-1468.
14. Sniegowski PD, Dombrowski PG, & Fingerman E (2002) Saccharomyces cerevisiae and Saccharomyces paradoxus coexist in a natural woodland site in North America and display different levels of reproductive isolation from European conspecifics. *FEMS Yeast Res* 1(4):299-306.